IEEE Access
Multidisciplinary ⋮ Rapid Review ⋮ Open Access Journal

Received October 15, 2020, accepted October 23, 2020, date of publication October 27, 2020, date of current version November 16, 2020.

Digital Object Identifier 10.1109/ACCESS.2020.3033981

Degree of Linear Polarization of Land Surfaces: Analyses Using POLDER/PARASOL Measurements

SIYUAN LIU[1], LEI YAN[1,3], (Senior Member, IEEE), AND BIN YANG[2], (Member, IEEE)

[1]Beijing Key Laboratory of Spatial Information Integration and 3S Application, Institute of Remote Sensing and Geographic Information System, School of Earth and Space Sciences, Peking University, Beijing 100871, China
[2]College of Electrical and Information Engineering, Hunan University, Changsha 410082, China
[3]Guangxi Key Laboratory of Remote Measuring System, Guilin University of Aerospace Technology, Guilin 541004, China

Corresponding author: Bin Yang (binyang@hnu.edu.cn)

This work was supported in part by the Natural Science Foundation of Hunan Province, China, under Grant 2019JJ50047, in part by the National Natural Science Foundation of China under Grant 41801227, and in part by the National Key Research and Development Program of China under Grant 2017YFB0503004.

ABSTRACT Polarized reflectance (R_p) and degree of linear polarization (DOLP) provide essential information about polarized characteristics of land surfaces. For a given target, DOLP determines the magnitude of R_p. It has been proved that DOLP can be used for some remote monitoring cases that cannot be well detected with either non-polarized or polarized reflectance. Several bidirectional polarization distribution function (BPDF) models have been proposed in the last several decades to reproduce the angular distribution of R_p, but much less attention has been devoted to modeling and analyzing of DOLP. In this study, the Nadal–Bréon BPDF model was transferred for calculating the DOLP of earth targets, and characteristics of DOLP were analyzed based on the modeling results. To evaluate the model's feasibility, two experiments were executed: a fitting and a *a priori* modeling. The results showed good correlations ($r > 0.9$) between estimated and measured DOLP when the model was fitted with POLDER/PARASOL (a space-borne multi-angle multi-spectral polarimetric sensor) measurements. An increase of accuracy from 490 nm to 865 nm for fitting modeling was achieved and the highest accuracy was found at 865 nm for both experiments, with overall relative root mean square errors of 1.1 and 1.3 for fitting and *a priori* modeling, respectively. Class-based free parameters can be used for the *a priori* model of DOLP. The dispersion of the target-based free parameters controls the correlation of the *a priori* modeling results. Moreover, the maximum DOLP was found to be strongly determined by the corresponding bidirectional reflectance factor for every surface type ($R^2 = 0.86$). This study provides an additional approach for obtaining DOLP from remote sensing platform and is helpful for studies of typical land surfaces.

INDEX TERMS Degree of linear polarization (DOLP), bidirectional polarization distribution function (BPDF), POLDER/PARASOL, BRDF-BPDF database.

I. INTRODUCTION

Polarized radiation of earth surface is caused primarily by specular reflection that occurs on ground targets [1]. Earth surface characteristics, such as roughness [2], water content [3] and biochemical and structural information of vegetation [4]–[7] can be retrieved with the help of either surface polarized reflectance (R_p) or degree of linear polarization (DOLP). On top of that, as a boundary condition, polarized characteristics of land surfaces are essential for retrieval of atmospheric properties, e.g. aerosol microphysical properties and the optical depth [8]–[10].

In the last several decades, study of angular distribution of R_p has been a hot topic, and several bidirectional polarization distribution function (BPDF) models have been proposed. These models can be broadly categorized as three types: physical [11], [12], semi-empirical [13]–[19] and neural-network-based [20]. Physical models have the best physical interpretation. However, they may require a set of biophysical parameters that are difficult to be obtained [12]. The neural networks-based models have been proven to be more accurate but they may require more intensive computation [20]. Semi-empirical models are easy-to-use

The associate editor coordinating the review of this manuscript and approving it for publication was Zhongyi Guo.

and usually produce satisfactory precision [21]. They are thus preferred in most cases. Semi-empirical models were proposed using measurements collected from various types of spectropolarimeters, e.g. the Diner Model using ground-based Multi-angle SpectroPolarimetric Imager (Ground MSPI) [14], the Waquet model using airborne polarimeter MICROPOL [16], the Litvinov model using Research Scanning Polarimeter (RSP) [15], the Nadal–Bréon [18], Maignan [17] and Xie-Cheng models [13] using space-borne POLarization and Directionality of Earth's Reflectances (POLDER). POLDER onboard the PARASOL satellite (POLDER/PARASOL) provided long-term polarization observations of land surfaces from 2005 to 2013. Thanks to the BRDF-BPDF database generated from POLDER/PARASOL measurements [22], much less effort is required for the BPDF modeling and its applications.

The above mentioned BPDF models were all proposed for modeling angular distribution of R_p over various land surfaces, whereas less attention has been dedicated to modeling DOLP and analyzing its characteristics. DOLP is critical for remote sensing using polarimetric techniques. On one hand, for a given target, DOLP indicates the proportion of polarized reflected radiation, i.e. DOLP determines the magnitude of R_p. For field measurements, due to DOLP's independence to the radiometer calibration and the incoming flux [11], the Stokes parameters should be measured and combined to obtain DOLP first, and R_p is obtained from product between bidirectional reflectance factor (BRF) and DOLP [5], [23]. On the other hand, unlike R_p, DOLP is wavelength-dependent, indicating its ability to reveal the polarized properties of the targets that are complementary to BRF. For example, DOLP shows different values among vegetation in different agronomic status [4], [7], [24]. Soybean canopy with and without water stress can be classified using DOLP but cannot be well detected only from BRF measurements [7], [12]. Corn canopy before and after flowering can be well discriminated at larger viewing angels using DOLP, whereas the two canopies share similar spatial distribution of R_p [12]. That is to say, DOLP can be used for some remote monitoring cases that cannot be dealt with using either BRF or R_p. Therefore, angular distribution modeling and analyses of DOLP is of great significance for both R_p's on-site acquisition and remote monitoring of key parameters of terrestrial ecosystem. The POLDER/PARASOL BRDF-BPDF database provides surface BRF and R_p, allowing to build such models and analyze the characteristics of DOLP.

The objectives of this article are thus: 1) to build a model for estimation of surface DOLP using the Nadal–Bréon BPDF model based on POLDER/PARASOL measurements; 2) to evaluate the accuracy of the DOLP model using different experiments; and 3) to analyze the characteristics and potential applications of DOLP.

The paper is organized as follows. Firstly, Section 2 gives the introduction of the database, generation process of DOLP and the Nadal-Bréon BPDF model. Then Section 3 presents two experiments involving fitting and *a priori* modeling and their results. Section 4 presents a discussion about the model's performance and the characteristics of DOLP, and finally, Section 5 gives conclusions and prospects of this study.

TABLE 1. Statistics of selected polder/parasol observations and targets.

IGBP class ID	IGBP class	Observations	Targets
01	Evergreen Needleleaf Forest	40800	564
02	Evergreen Broadleaf Forest	33868	551
03	Deciduous Needleleaf Forest	35986	536
04	Deciduous Broadleaf Forest	43075	595
05	Mixed Forest	40112	581
06	Closed Shrubland	38431	341
07	Open Shrubland	87052	599
08	Woody Savannas	42984	556
09	Savannas	47740	589
10	Grassland	70778	599
11	Permanent Wetlands	33180	553
12	Croplands	58557	575
13	Urban and Built-up	26547	515
14	Cropland/Natural Vegetation Mosaic	40284	572
15	Snow and Ice	207028	554
16	Desert	102265	597
All		948687	8877

II. MATERIALS AND METHODS

A. POLDER BRDF-BPDF DATABASE

The data used in this study are from a new version of the POLDER/PARASOL BRDF-BPDF database [22], which includes surface BRF and R_p of 16 International Geosphere Biosphere Programme (IGBP) classes. The data are from the year 2008 and guarantee good continuity and quality of the observations [22]. This is the latest and most widely used database for modeling of land surface polarization and related studies [4], [13], [20], [21]. The database contains monthly and yearly datasets. In the monthly dataset, 50 targets with the highest quality of atmospheric correction in each month were provided. It thus contains 600 globally distributed targets for each IGBP class. In the yearly dataset, the same best 50 targets over the year were selected for 12 months. In this study we used the monthly dataset because of its better quality [22]. In the database, surface BRF for six spectral bands from 490 to 1020 nm (i.e. 490nm, 565 nm, 670 nm, 765 nm, 865 nm and 1020 nm) as well as surface R_p at 865 nm were atmospherically corrected. The dataset is freely available from the PANGAEA website (doi:10.1594/PANGAEA.864090).

It is notable that observations for which R_p had a filled value (indicating missing observation) are excluded from the monthly dataset. Moreover, observations with Aero bigger than 5 were also excluded in order to suppress aerosol effects [21]. Here, Aero represents the level of aerosol load of observations ranging from 0 (for minimum) to

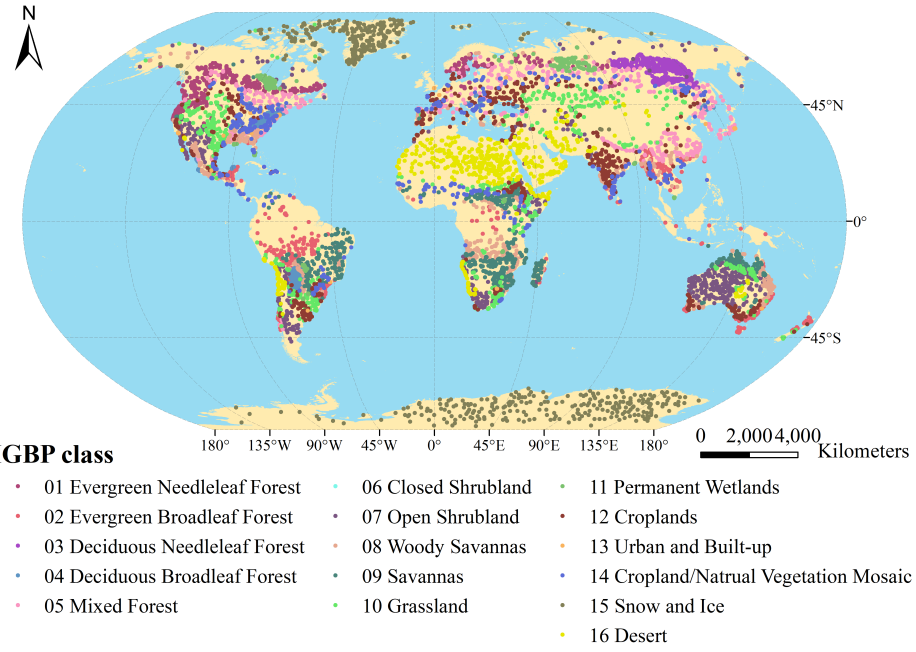

FIGURE 1. Global distribution of the selected targets of 16 IGBP classes in the monthly POLDER/PARASOL measurement database.

15 (for maximum) [22]. The number of selected targets of each IGBP class are consequently lower than 600, as seen in Table 1. The global distribution of the selected targets is shown in Fig. 1.

B. GENERATION OF THE DEGREE OF LINEAR POLARIZATION (DOLP)

DOLP describes the percentage of linearly polarized wave in a specific beam of radiation. The POLDER polarispectrometer measured the Stokes vectors $[I, Q, U]$ of the detected radiance, where I represents the total radiance, and Q and U quantify linearly polarized radiance with specific angles to a fixed reference plane [17], [22]. If we take the scattering plane as the reference plane, Q denotes the fraction of radiation that polarizes perpendicularly or parallel to the reference plane, and U represents the fraction of radiation that polarizes obliquely to the reference plane. Moreover, the sign of Q and U denotes the polarizing directions. For example, positive and negative Q denotes the polarizing direction perpendicular and parallel to the reference plane, respectively. In most cases, the reflected radiation polarizes light perpendicularly to the scattering plane, making Q negative and U negligible compared to I and Q [17]. The DOLP can be thus described by the ratio between $-Q$ and I:

$$DOLP = \frac{-Q}{I} \tag{1}$$

For POLDER measurement, BRF and R_{p} are defined as:

$$BRF = \frac{\pi I}{E_0 cos\theta_s} \tag{2}$$

and

$$R_p = \frac{-\pi Q}{E_0 cos\theta_s} \tag{3}$$

respectively, where $\boldsymbol{E_0}$ indicates the top of atmospheric solar irradiance, and $\boldsymbol{\theta_s}$ is the sun zenith angle. With these two parameters, the DOLP of the earth surface can be thus derived from surface BRF and R_{p} provided in the database:

$$DOLP = \frac{R_p}{BRF} \tag{4}$$

Theoretically, DOLP ranges from 0 to 1, so observations with "noisy" DOLP bigger than 1were further excluded in the dataset. It is notable that around 7% of the observations gave negative polarized reflectance, leading to negative DOLPs. The negative DOLPs are at a very small magnitude not larger than 0.005, and they correspond to the above-mentioned parallel-polarizing observations.

The above-mentioned scheme produces DOLP at 865 nm. To produce DOLP for other bands of the POLDER instrument, we applied a widely used hypothesis, suggesting that the surface R_{p} is spectrally invariant, i.e. it rarely changes with wavelengths from the visible to the near infrared spectral region [16], [18], [24]. Consequently, DOLP for any band can be easily derived from the ratio of R_{p} at 865 nm and BRF in the corresponding band. It can be easily found from Fig. 2 that, similarly to R_{p} [21], the DOLP of reflected radiation shows an obvious anisotropic spatial distribution that is symmetric about the principle plane, and bigger phase angles (the angles between observation and illumination) yield bigger DOLPs. Highest DOLPs always occur at the forward scattering direction along the principle plane when

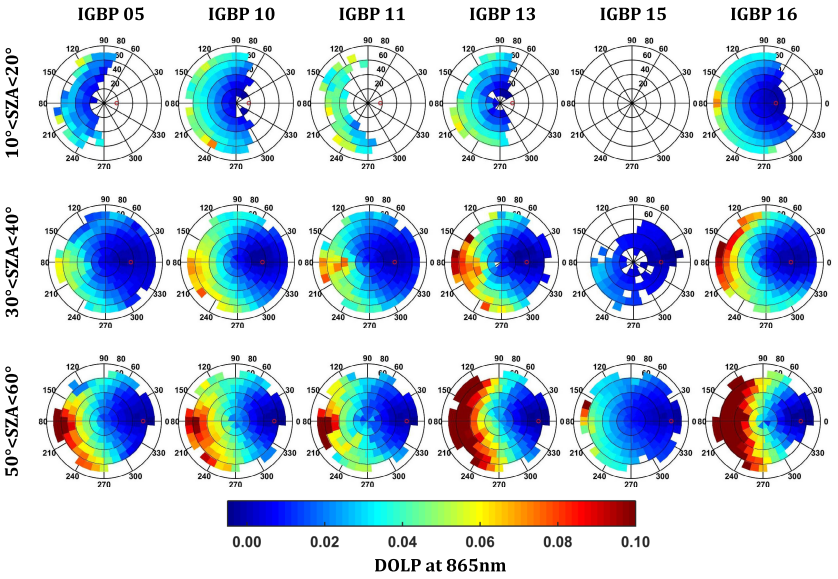

FIGURE 2. Polar plots of the measured DOLP at 865 nm for six representative earth surfaces, i.e. mixed forest (IGBP 05), grassland (IGBP 10), permanent wetlands (IGBP 11), urban and built-up (IGBP 13), snow and ice (IGBP 15) and desert (IGBP 16). The black circles represent different view zenith angles at 20 degrees intervals whereas the black lines represent relative azimuth angles, at 30 degrees intervals, with respect to the direction of solar incidence marked with small red circles. The three rows represent different sun zenith angles (SZA). The color bar ranges from -0.005 to 0.10. The DOLP value in each angular bin is the average of all selected measurements in each IGBP class within the corresponding sun-sensor geometry.

viewing angle is large (>60°), and lowest DOLPS (with negative values) are around the back scattering area near to the solar incident direction. Such characteristics can also be found in other wavelengths (not shown).

C. DOLP MODELING

DOLP shows a similar angular distribution pattern with R_p(Fig. 2), which lays a possibility of using existing semi-empirical BPDF models for DOLP modeling. Among several widely used semi-empirical BPDF models mentioned above, the Nadal–Bréon model has been reported to give relatively higher accuracy [13], [17], [21]. It also served as the algorithm for aerosol properties retrieval over land surfaces using POLDER measurements [17], [18]. Thus, the Nadal–Bréon model is considered in this study for reproducing and analyzing the angular distribution of DOLP.

The Nadal–Bréon BPDF model was proposed for accurate estimation of R_p for four major surface types, i.e. desert, shrubland, forest and low vegetation. It was built using two free parameters, $\boldsymbol{\rho}$ and $\boldsymbol{\beta}$ [18]:

$$R_p(\theta_s, \theta_v, \varphi) = \rho(1 - exp(-\beta \frac{F_p}{(cos\theta_s + cos\theta_v)})) \quad (5)$$

where F_p is the polarized component of Fresnel function [24], θ_s and θ_v the sun zenith angle and view zenith angle, respectively. F_p represents the specular reflection process that generates polarization, and it is a function of incident angle, $\boldsymbol{\alpha}$, and the refractive index of the land surface, N. It is written as:

$$F_p(\alpha, N) = \frac{1}{2}\left[\left(\frac{Ncos\alpha' - cos\alpha}{Ncos\alpha' + cos\alpha}\right)^2 - \left(\frac{Ncos\alpha - cos\alpha'}{Ncos\alpha + cos\alpha'}\right)^2\right] \quad (6)$$

Here, N is fixed to 1.5 for land surface, which is commonly accepted [18], [20], [24]. α' represents the refractive angle and it can be related to $\boldsymbol{\alpha}$ through:

$$sin(\alpha) = Nsin(\alpha') \quad (7)$$

α can be simply related to the scattering angle, γ, through $\alpha = (\pi - \gamma)/2$. For a given sun-sensor geometry, γ is defined as the angle between the solar incident direction and the reflected light direction, and can be calculated as:

$$cos\gamma = -cos(\theta_s)\, cos(\theta_v) - sin(\theta_s)\, sin(\theta_v)\, cos(\varphi) \quad (8)$$

where φ is the relative azimuth angle between the solar and view directions.

Equation (5) was built based on a non-linear relationship between R_p and the Fresnel factor, $F_p(\alpha)/(cos\theta_s + cos\theta_v)$ [18]. Analogously, by plotting the Fresnel factor and DOLP at 865 nm, similar relationships can be obtained, as shown in Fig. 3. Cases using other bands are similar to those at 865 nm, and are not illustrated here. As such, the Nadal–Bréon BPDF model can be migrated for DOLP modeling as:

$$DOLP(\theta_s, \theta_v, \varphi, \lambda) = \rho(\lambda)(1 - exp(-\beta(\lambda) \frac{F_p}{(cos\theta_s + cos\theta_v)})) \quad (9)$$

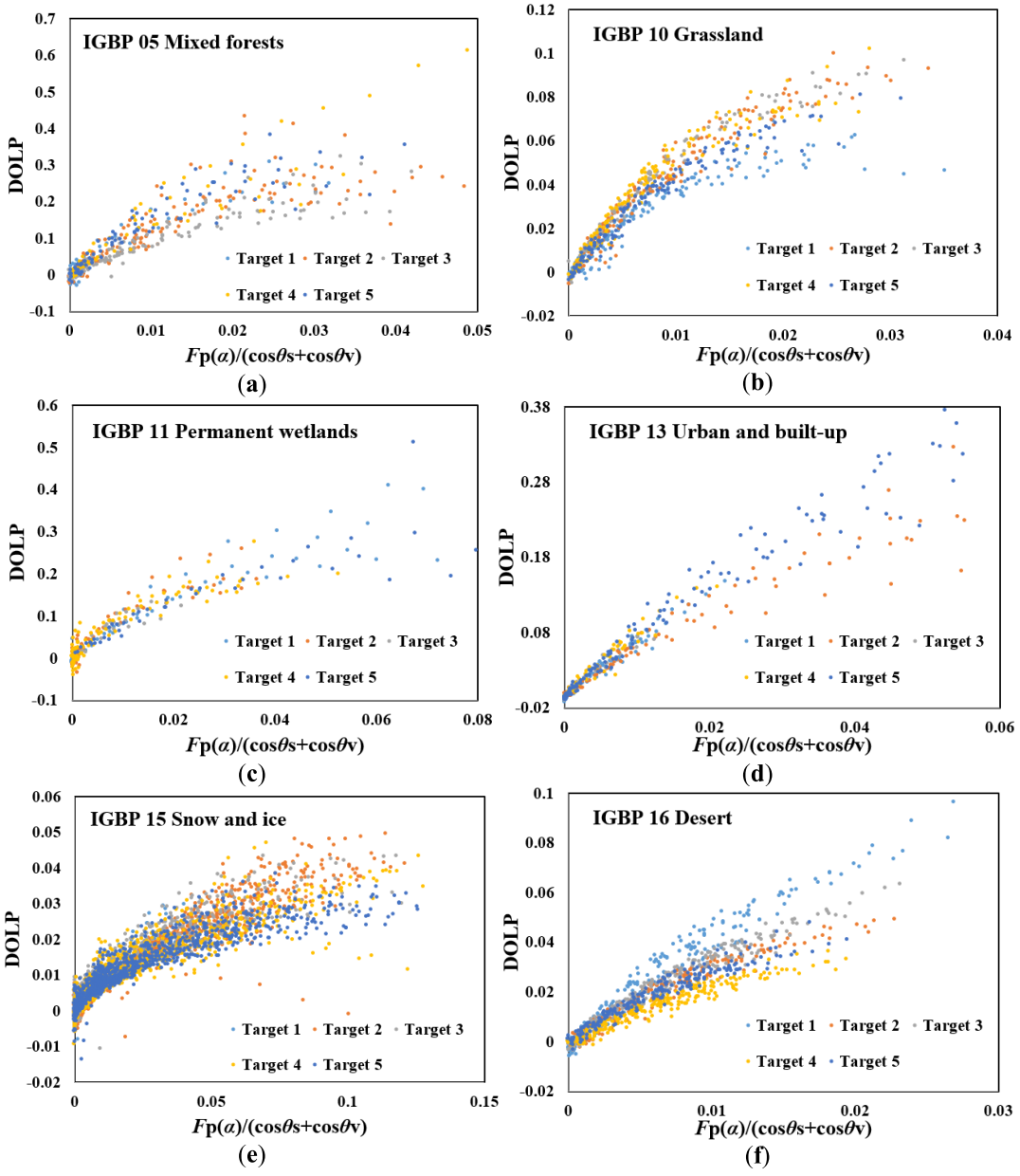

FIGURE 3. Relationship of POLDER-measured DOLP at 865 nm and the Fresnel factor, $F_P(\alpha)/(\cos\theta_S+\cos\theta_V)$, for six representative IGBP classes, i.e. (a) mixed forest (IGBP 05); (b) grassland (IGBP 10); (c) permanent wetlands (IGBP 11); (d) urban and built-up (IGBP 13); (e) snow and ice (IGBP 15) and (f) desert (IGBP 16). Five arbitrary targets in each IGBP class were selected to show such relationships.

Here, ρ controls the saturation value of the function whereas $\rho\beta$ indicates the slope of the linear relationship when DOLP is relatively small. Note that ρ and β are wavelength-dependent, which is different from those in equation (5). Moreover, ρ and β are target-based parameters as they are calibrated from observations of single targets.

III. EXPERIMENTS AND RESULTS

In order to evaluate the performance of the DOLP model, assessments of accuracy of fitting results (the results of model fitted on every single target), and *a priori* modeling results (the results of model with *a priori* free parameters when no polarization measurement exists), were conducted. Given that the calculated DOLP varies with wavelength, i.e. it mostly ranges between 0 and 0.1 at 865 nm and between 0 and 0.3 in the visible bands (Fig. 4), the relative root mean square error (RRMSE) which describes the relative bias between modeled and measured values was used to intercompare the model performance over different bands. Moreover, the correlation coefficient (r) of measured and modeled DOLP was also applied. Note that r shows how well the estimation and

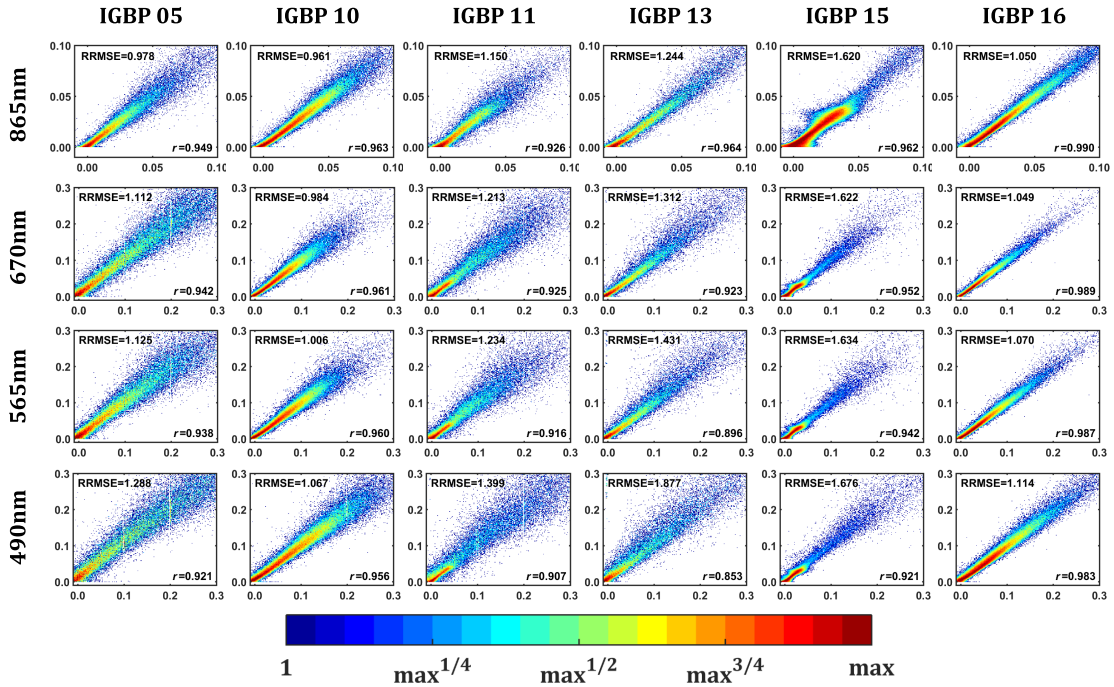

FIGURE 4. Scatter plots of measured versus modeled DOLP of six representative IGBP classes and four visible and near infrared bands of POLDER/PAROSOL. The range of x (measured) and y (modeled) is from -0.01 to 0.1 for 865 nm and from -0.01 to 0.3 for 670nm, 565nm and 490nm. The $100\times$root mean square error (RMSE) and correlation coefficient (r) of modeled and measured DOLP are given at the upper left and lower right corner of each plot, respectively. Note that the color in each bin represents the number of scatters on a logarithmic scale, so the warmer colored bins indicate much more scatters than cooler ones.

measurement are correlated to a specific line, but not necessarily to the 1:1 line.

A. FITTING RESULTS

In this part, the model was best fitted over every target per band and per IGBP class, and hundreds of sets of target-based ρ and β were obtained to calculate the modeled DOLP. Scatter plots of modeled against measured DOLPs of six representative IGBP class at 4 bands centered at 865 nm, 670 nm, 565 nm and 490 nm were illustrated in Fig. 4, and the corresponding statistics for all 16 classes are listed in Table 2.

According to Fig. 4 and Table 2, the modeled DOLP correlate well with the measurement along the 1:1 line, generally with r bigger than 0.9. The best correlated results were mostly found at 865 nm, except for IGBP 01, 03, 08, and 14 whose highest r were found at 670 nm. Analogously, the best fitting results with lowest RRMSE were produced at 865 nm except for IGBP 16. Overall, 865 nm appears to be the best band for fitting experiment, with highest overall r of 0.96 and lowest overall RRMSE of 1.15. The relatively worst fittings were found at 490 nm for all IGBP classes. There is a slight decrease in RRMSE of fitting results with the increase in wavelength from 490 nm to 865 nm, regardless of whether all classes were separated or combined (also see Fig. 6). Among the 16 IGBP classes, desert (IGBP 16) yielded the best correlation (with r bigger than 0.98 for all bands) between modeled and measured DOLP. This may be due to the high homogeneity of the target pixel with the size of 6×7 km width of the POLDER image, which rarely happens in other land surface type except IGBP 15, i.e. ice and snow. But ice and snow gave quite different optical properties compared with other surface types [19], which somewhat influenced the model's reproduction and made IGBP 15 yield the highest RRMSE among all surface types. Additionally, urban area (IGBP 13) also showed relatively high modeling error compared with other classes, which may be due to the smaller quantity of observations and the unique polarized features of the built-up areas.

B. A PRIORI MODELING RESULTS

Most of the remote sensing instruments are not equipped with polarimetric sensors. Nevertheless, *a priori* parameters derived from polarized observations can be utilized in empirical models to reproduce the polarized characteristics of the land surfaces. As proposed in [17] and utilized in [21], given hundreds of sets of target-based free parameters, i.e. ρ and β, per IGBP class and per band in section 3.1, their median values were chosen as representative *a priori* parameters, i.e. class-based parameters, for each corresponding surface type and for each band (listed in Table 3). Using the listed class-based *a priori* parameters, DOLP at a given band of a given surface type can be calculated using Equation (9) with specified sun-sensor geometry. The accuracy of the *a priori* modeling results are listed in Table 4.

TABLE 2. Accuracy of fitting results (*r* and RRMSE) for four bands and 16 IGBP classes. The best indices of each IGBP class are shown in ***Bold Italic***.

	490nm		565nm		670nm		865nm	
IGBP class ID	*r*	RRMSE	*r*	RRMSE	*r*	RRMSE	*r*	RRMSE
01	0.911	1.346	0.914	1.163	***0.921***	1.142	0.906	***1.026***
02	0.921	1.154	0.937	1.015	0.943	1.001	***0.943***	***0.877***
03	0.939	1.347	0.947	1.203	***0.947***	1.224	0.937	***1.131***
04	0.927	1.188	0.938	1.037	0.942	1.035	***0.954***	***0.926***
05	0.921	1.288	0.938	1.125	0.942	1.112	***0.949***	***0.978***
06	0.945	1.016	0.954	0.924	0.964	0.877	***0.969***	***0.853***
07	0.964	1.040	0.975	0.965	0.979	0.924	***0.979***	***0.919***
08	0.941	1.103	0.953	0.952	***0.959***	0.944	0.947	***0.852***
09	0.944	1.028	0.950	0.934	0.956	0.899	***0.960***	***0.863***
10	0.956	1.067	0.960	1.006	0.961	0.984	***0.963***	***0.961***
11	0.907	1.399	0.916	1.234	0.925	1.213	***0.926***	***1.150***
12	0.955	1.107	0.961	1.033	0.965	1.008	***0.967***	***0.963***
13	0.853	1.877	0.896	1.431	0.923	1.312	***0.964***	***1.244***
14	0.939	1.095	0.951	0.975	***0.955***	0.963	0.951	***0.884***
15	0.921	1.676	0.942	1.634	0.952	1.622	0.962	***1.620***
16	0.983	1.114	0.987	1.070	0.989	1.049	***0.990***	1.050
All	0.944	1.301	0.952	1.204	0.957	1.183	***0.962***	***1.145***

TABLE 3. ***A priori*** free parameters for 16 IGBP classes at different wavelength.

	490nm		565nm		670nm		865nm	
IGBP class ID	ρ	β	ρ	β	ρ	β	ρ	β
01	0.316	46.378	0.222	39.239	0.250	42.527	0.063	33.706
02	0.357	65.816	0.281	42.769	0.337	53.643	0.048	38.143
03	0.266	49.343	0.183	43.807	0.203	45.064	0.068	36.894
04	0.356	58.102	0.264	46.060	0.288	49.996	0.083	41.627
05	0.460	47.123	0.333	38.048	0.369	43.019	0.096	30.259
06	0.267	62.975	0.186	57.766	0.143	53.681	0.072	57.745
07	0.303	46.875	0.204	44.470	0.141	44.664	0.081	51.856
08	0.422	49.882	0.289	41.762	0.319	44.211	0.071	43.866
09	0.316	61.047	0.213	54.031	0.203	52.687	0.057	59.978
10	0.251	52.775	0.173	51.260	0.142	52.098	0.068	59.170
11	0.354	48.126	0.231	44.455	0.258	44.890	0.064	44.121
12	0.299	55.068	0.207	51.104	0.201	50.123	0.073	51.933
13	0.824	15.890	0.631	14.962	0.487	18.766	0.144	27.907
14	0.383	51.664	0.259	46.255	0.294	48.351	0.067	45.195
15	0.034	34.361	0.034	34.760	0.035	35.554	0.037	36.744
16	0.222	43.915	0.140	42.010	0.097	42.459	0.082	42.009

Coincident with the fitting results, 865 nm gives generally the most accurate *a priori* modeling of DOLP with overall RRMSE of 1.32, while IGBP 04, 05 and 12 were best estimated at 565 nm and IGBP 06 at 670 nm. However, differences regarding r were noticed in Table 4 compared with the fitting results: the highest r for most of the classes and for the entirety were yielded at 565 nm, whereas for IGBP 01, 03, 11, 13 and 15, 865 nm was the best correlated band.

IV. DISCUSSION

DOLP of land surfaces provides critical information of surface optical properties and it determines the magnitude of polarized reflectance. For a given target at a given wavelength, the angular distribution of DOLP shows significant anisotropic features (Fig. 2), which is similar to R_p. In this study, the Nadal–Bréon BPDF model with two free parameters (Equation (9)) was transferred to reproduce the angular variations of DOLP (Fig. 3). The model was calibrated and validated based on polarimetric observations from a widely used POLDER BRDF-BPDF database (Fig. 1). Class-based free parameters (Table 3) for all IGBP classes of common bands were produced as inputs to the *a priori* model for DOLP estimation. The model yields high precision and the accuracy peaks at 865 nm (Table 2 and Table 4).

TABLE 4. Accuracy of a priori modeling results (r and RRMSE) for four bands and 16 IGBP classes. The best indices of each IGBP class are in bold Italic s.

	490nm		565nm		670nm		865nm	
IGBP class ID	*r*	RRMSE	*r*	RRMSE	*r*	RRMSE	*r*	RRMSE
01	0.690	4.089	0.705	2.606	0.681	2.978	***0.716***	***1.203***
02	0.791	1.271	***0.804***	1.212	0.791	1.345	0.751	***1.126***
03	0.496	6.367	0.569	3.869	0.496	4.419	***0.764***	***1.275***
04	0.856	1.304	***0.874***	***1.050***	0.814	1.342	0.810	1.211
05	0.835	1.414	***0.846***	***1.225***	0.818	1.356	0.802	1.366
06	0.874	1.086	0.895	0.954	***0.905***	***0.926***	0.871	0.965
07	0.850	1.138	***0.896***	1.042	0.875	1.017	0.890	***0.982***
08	0.820	1.260	***0.840***	1.072	0.802	1.272	0.774	***1.071***
09	0.849	1.167	***0.857***	1.032	0.820	1.154	0.756	***0.953***
10	0.856	1.201	***0.877***	1.113	0.818	1.210	0.838	***1.068***
11	0.589	8.408	0.627	5.004	0.625	5.419	***0.718***	***1.490***
12	0.872	1.284	***0.888***	***1.170***	0.823	1.354	0.826	1.181
13	0.725	2.548	0.802	2.044	0.815	1.967	***0.871***	***1.422***
14	0.855	1.292	***0.874***	1.147	0.820	1.625	0.821	***0.999***
15	0.398	1.868	0.473	1.833	0.532	1.821	***0.706***	***1.798***
16	***0.850***	1.308	0.817	1.211	0.795	1.197	0.782	***1.165***
All	0.821	2.567	***0.834***	1.832	0.818	1.983	0.797	***1.315***

TABLE 5. Proportion of DOLP bigger than 1 that were excluded from the database per IGBP class and per waveband.

IGBP class ID	490 nm	565 nm	670 nm	765 nm	865 nm	1020 nm
01	0.4%	0.1%	0.2%	0	0	0
02	2.0%	0.3%	0.5%	0	0	0
03	0.2%	0	0.1%	0	0	0
04	0.3%	0	0	0	0	0
05	1.6%	0.4%	0.5%	0	0	0
06	0.1%	0	0	0	0	0
07	0.2%	0	0	0	0	0
08	2.5%	0.4%	0.3%	0	0	0
09	0.6%	0.1%	0	0	0	0
10	0.1%	0	0	0	0	0
11	1.6%	0.3%	0.2%	0	0	0
12	0.3%	0	0	0	0	0
13	3.1%	1.2%	0.7%	0	0	0
14	0.7%	0.1%	0	0	0	0
15	0.1%	0	0	0	0	0
16	0	0	0	0	0	0
All	0.6%	0.1%	0.1%	0	0	0

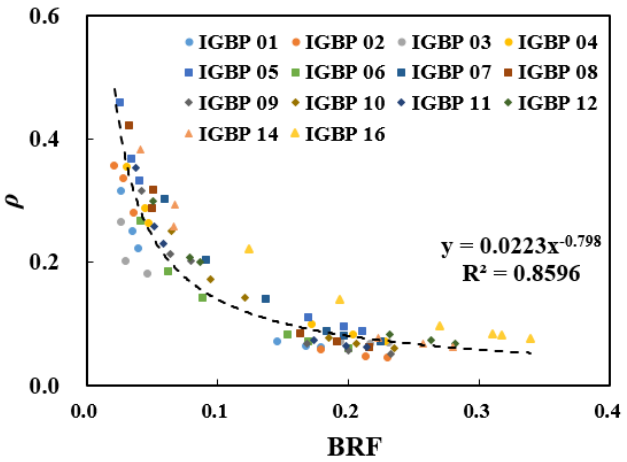

FIGURE 5. Scatter plot of ρ and surface BRF at six bands, i.e. 490nm, 565 nm, 670 nm, 765 nm, 865 nm and 1020 nm, for 14 IGBP classes excluding IGBP 13 (urban and built-up) and 15 (ice and snow). Each BRF is the average of all selected measurements in a given IGBP class within a specified sun-sensor geometry: sun zenith angle from 25 to 35 degrees, view zenith angle from 35 to 45 degrees and relative zenith angle from 175 to 185 degrees.

It is notable that in the data pre-processing of the POLDER BRDF-BPDF database, observations with DOLP bigger than 1 were excluded. As seen in Table 5, the "noisy" items only occurred at visible wavebands (from 490 nm to 670 nm) and took up a very small part of the data, with a proportion mostly lower than 1%, No "noisy" item occurred in near-infrared wavebands (from 765 nm to 1020 nm). The noise was generated when DOLP was calculated from the ratio of the polarized reflectance and BRF of land surfaces. The visible wavebands are the spectral region where some land surfaces (e.g. vegetated surfaces) absorb radiation, and the BRF of these surfaces consequently shows relatively low values. These values can be occasionally interfered by noise and yield very small values near to zero, leading to very large DOLPs (sometimes can be infinite). These abnormal values would largely influence the model performance, so they were removed from the dataset.

The free parameter ρ reflects the maximum DOLP of a given surface type at a given wavelength. Previous studies have found a negative relationship between DOLP and BRF given that R_p is insensitive to wavelength [11], [25]. Analogously, Fig. 5 plotted class-based ρ with the BRF of corresponding classes. We calculated the average BRF of all observations within a specified sun-sensor geometry at six bands for all IGBP classes except IGBP 13 (urban and built-up) and 15 (ice and snow). IGBP 13 was excluded because urban area shows complex features and

R_p of different city targets with different complexity vary greatly [13]. Snow and ice (IGBP 15) is distributed mainly at the poles and thus does not have the required observations satisfying this geometry. A strong negative correlation between ρ and BRF was found for each of the IGBP classes and this relationship can be described by a negative power function, as shown in Fig. 5. It is interesting that this relationship is stable regardless of the IGBP class, with quite high R^2 of 0.86 when all classes are taken into consideration. Note that the specified sun-sensor geometry would have an impact on the relationship. It suggests that once the BRF of an arbitrary surface type (except urban area and snow/ice) is obtained, the maximum DOLP at different wavelengths could be estimated. It provides an approach for estimation of the maximum polarization the land surface can produce using remote sensing, based on which the polarized properties of specific targets can be obtained and utilized for further analyses.

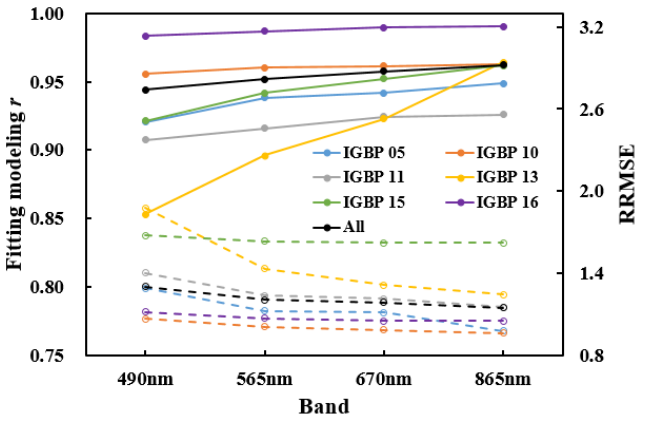

FIGURE 6. Variation of fitting results accuracy for 6 representative IGBP classes from 490 nm to 865 nm. Correlation coefficients (*r*, solid lines) correspond to the left *y* axis whereas the RMSE (×100, dashed lines) correspond to the right *y* axis.

An increase of fitting accuracy from 490 nm to 865 nm was obtained, as shown in Fig. 6 and Table 2. This can be attributed to two reasons. First, the hypothesis that R_p is spectrally invariant is not always satisfied. As mentioned in previous studies [1], [11], it has been tested in situ with high spatial resolution instruments that there is a slight increase in R_p when the wavelength changes from visible to near infrared band (a departure within 8% from the hypothetical slope of 1 of R_p in visible and near infrared bands), especially for vegetation (a departure of about 30%). This is because the leaf interior and wax layer on the leaf surface may change the polarization behavior at some wavelengths [1]. This suggests that, the real R_p at visible bands, i.e. 490 nm, 565 nm and 670 nm, is not exactly but slightly lower than the R_p at 865 nm, inducing errors into the model in the visible bands. Using the R_p at 865 nm certainly made the DOLP at 865 nm more accurate than for other bands. This explains the increasing accuracy from visible to near infrared on one hand.

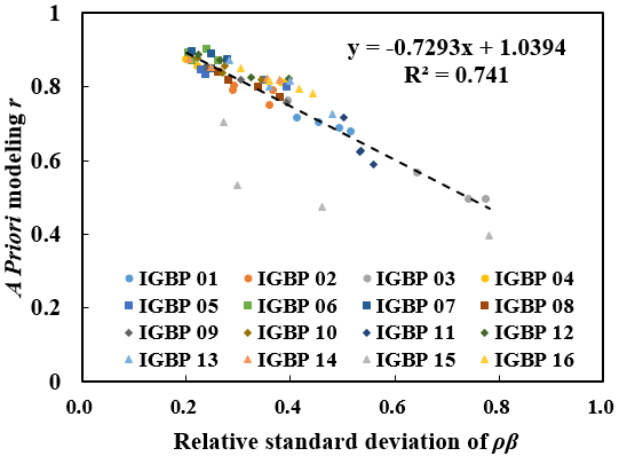

FIGURE 7. Relation of the correlation coefficient (*r*) of the *a priori* modeling and the relative standard deviation of $\rho\beta$.

On the other hand, the atmospheric effect is greater and more difficult to correct at shorter wavelengths [22]. This makes the calibrated BRF of visible bands, in the database, relatively less accurate than that at 865 nm. This is also the reason why only R_p at 865 nm is provided in the database. These two factors, surface R_p and surface BRF, explain the fitting accuracy variation from the visible to the near infrared bands. The free parameters derived at 865 nm in Table 3 are thus recommended for accurate estimation of DOLP.

The reasons above reflect a potential criticism of DOLP modeling process, i.e. the measured DOLP in this study was calculated from the ratio of R_p and BRF, and thus with errors derived from the detection, calibration and correction process of both surface BRF and R_p. This makes the applied model sensitive to the precision of R_p and BRF in the database, especially for visible wavelengths where the BRF is smaller (e.g. for vegetation) and thus noisier compared with that of the near infrared bands. Therefore, increased model performance requires higher data precision.

For *a priori* modeling experiment, the lowest RRMSE was mostly found at 865 nm whereas the highest r between modeled and measured DOLP was mostly seen at 565 nm. In fact, as the median value of the target-based parameters was used to represent the class-based parameter of *a priori* models, the dispersion of target-based parameters determines the correlation between modeled and measured DOLP. Therefore, the more dispersed the target-based parameters are, the less the median value can represent the entirety, and the worse the modeled and measured values correlate, leading to lower r in the *a priori* modeling results. Consequently, the relative standard deviation (RSD) was utilized to describe the dispersion of the target-based parameters, ρ and β, and their multiplication, $\rho\beta$. RSD was calculated as:

$$RSD = \frac{STD(para)}{\overline{para}} \times 100\% = \frac{\sqrt{\frac{\sum_{i=1}^{n}(para_i - \overline{para})^2}{n-1}}}{\overline{para}} \times 100\% \quad (10)$$

where $STD(para)$ and $\overline{para}$ represent the standard deviation and the average of the target-based parameters in a given IGBP class, respectively. A highly negative correlation can be found in Fig. 7 when r of the *a priori* modeling and RSD of $\rho\beta$ were scattered for all IGBP classes. Scatters of IGBP 15 (ice and snow) are biased from those of other surface types, indicating a relatively less correlated results of this class. It is because ice and snow show different optical properties with other types of earth targets and they may require a unique model to describe their polarization characteristics [19]. The R^2 of the regression line is 0.741. Such high correlated relationship cannot be found in relationships between r and either ρ ($R^2 = 0.503$) or β ($R^2 = 0.001$). It indicates that the correlation of the *a priori* model performance is mainly determined by the dispersion of $\rho\beta$. It can be explained by the fact that most of the DOLP are concentrated in the linear-relationship area of the scatter plots between DOLP and $F_p/(\cos\theta_s+\cos\theta_v)$ (Fig. 3), so the dispersion of $\rho\beta$ controlling the slope of the linear relationship has a great influence on the model's performance.

This study remains unable to reproduce negative DOLP values that indicate the reflected polarization parallel to the scattering plane when scattering angle is close to 180°. This is because the Nadal–Bréon BPDF model (Equation (9)) assumes a positive R_p (and consequently positive DOLP) and thus cannot fit the negative values, which take up nearly 7% of all observations. This drawback has existed in all semi-empirical BPDF models, but can be solved in models based on machine leaning techniques, e.g. GRNN-based BPDF model [20]. That is because neural network-based models take positive and negative values as training samples and allocate the possibilities of all these samples. In the future, machine learning-based models could be further developed for DOLP modeling to reproduce the negative DOLP in the back-scattering area.

In general, the Nadal–Bréon BPDF model provides a good accuracy for DOLP estimation, with acceptable errors in both fitting and a priori modeling results. The feasibility is further confirmed when the model's accuracy is compared with that of current BPDF models for R_p modeling. Table 6 illustrated the performance, in terms of correlation coefficient between modeled and measured values, of Nadal-Bréon model for R_p and DOLP modeling. Overall, the DOLP model slightly outperformed the R_p model for fitting modeling, whereas the R_p model gave more correlated results than DOLP model for *a priori* modeling. Nevertheless, the difference was not great, so it can be summarized that the DOLP model gave a competitive performance to the R_p model. The Nadal–Bréon BPDF model was utilized in this study, for its consistently relatively high precision of surface R_p modeling for most of the IGBP classes, when models were fitted against different datasets [17], [21].

A priori parameters obtained in this study (Table 3) are key parameters for land surface remote monitoring that is based on the polarized characteristics. As many space-borne sensors are non-polarimetric, only optical non-polarized spectral features can be detected using the data acquired from these sensors. However, *a priori* parameter provides an option to estimate DOLP of arbitrary types of land surfaces, by combining with the Fresnel function which can be directly obtained from the sun-sensor geometry of the sensor. The *a priori* parameters in this study were derived from the POLDER/PARASOL measurements with a spatial resolution of 6 × 7 km, it thus makes more sense to apply these parameters to sensors with moderate or coarse resolution, e.g. Moderate-resolution Imaging Spectroradiometer (MODIS) and Advanced Very High Resolution Radiometer (AVHRR). Although the spatial resolution of these radiometers ranges from 200 meters to 1 kilometer, the *a priori* parameters obtained in this study are applicable because the dataset we used for modeling guaranteed the homogeneity of every POLDER pixel (>75% of the pixel is the same surface type). This study thus provides an approach to obtain and analyze the DOLP of land surfaces on moderate to coarse scale. With the usage of the coarse-scale DOLP, further investigations, e.g. the capability of DOLP for classification of vegetation with different structural parameters and different agronomic status [7], [12], [24], should be conducted in the future.

Furthermore, applying the model to a finer scale (e.g. meter-level resolution) thus requires further investigation using more experimental data, e.g. in-situ measurements. Moreover, other BPDF models or improved versions using other nonlinear estimators describing the relationship between DOLP and the Fresnel factor can be investigated for further improvement of the DOLP modeling in future studies [26]. Surface DOLP from other platforms e.g. airborne AirMSPI [14], AMPR [27], MICROPOL [16], RSP [28], or space-borne DPC/GF-5 [29] and the

TABLE 6. Comparison of the modeling correlation coefficient between the Nadal-Bréon model for polarized reflectance (R_p) and DOLP. The correlation coefficient for R_p modeling is from reference [21].

IGBP class ID	Fitting modeling		*A priori* modeling	
	for R_p	for DOLP	for R_p	for DOLP
01	0.898	0.906	0.730	0.716
02	0.925	0.943	0.746	0.751
03	0.935	0.937	0.850	0.764
04	0.923	0.954	0.831	0.810
05	0.922	0.949	0.813	0.802
06	0.965	0.969	0.896	0.871
07	0.977	0.979	0.913	0.890
08	0.927	0.947	0.795	0.774
09	0.952	0.960	0.827	0.756
10	0.955	0.963	0.856	0.838
11	0.940	0.926	0.835	0.718
12	0.955	0.967	0.886	0.826
13	0.934	0.964	0.900	0.871
14	0.933	0.951	0.851	0.821
15	0.948	0.962	0.916	0.706
16	0.987	0.990	0.962	0.782
All	0.942	0.962	0.850	0.797

forthcoming 3MI/EPS-SG [30], can also be further utilized to build DOLP models for all available wavelengths, to better serve studies on ground polarized characteristics and their further applications in terrestrial ecosystem, climate change and atmospheric monitoring.

V. CONCLUSION

DOLP plays an important role in studies of polarized properties of vegetation, urban and snow. This article reproduced the angular distribution of DOLP using transferred Nadal–Bréon BPDF model. The model was validated using the POLDER/PARASOL measurements, and showed high precision for the two experiments, i.e. fitting and a priori modeling. Parameters derived at 865 nm are recommended to be used to estimate DOLP. A negative correlation between the DOLP and BRF helps to obtain maximum polarization information of land surface using non-polarized detection. This modeling process is sensitive to the error of R_p and BRF, leading to an increase of estimation accuracy from short to long wavebands. Data with higher quality may lead to a more accurate modeling of DOLP at shorter wavelengths.

This study helps to provide additional information for study of polarization characteristics of land surfaces. It provides a means for estimating DOLP directly from remote sensing platforms with or without polarimetric instruments. Field measurements aiming at building bidirectional DOLP distribution functions benefit the more accurate studies of polarization characteristics of earth targets [31], and this study contributes directly to such work. Moreover, this study serves for aerosol parameters retrieval over various land surfaces by providing the boundary conditions of the atmosphere [9]. Different from R_p, the spectrally variant property makes DOLP more informative and effective for remote sensing applications. The spectrally polarized feature of a given target given by DOLP varies inversely to the spectral features given by BRF. In this case, this study provides complementary information to compensate or enhance normal non-polarized remote sensing on the earth surface. For example, remote monitoring and classification of crop structure parameters [7], sunglint detection on oceanic oil slicks [32], and detection of land surface types with varying contamination [33] have been proven effective using DOLP.

ACKNOWLEDGMENT

The authors would like to thank the Centre National d'Etudes Spatiales (CNES) for preprocessing the POLDER/PARASOL data and making the BPDF-BRDF database publicly available.

REFERENCES

[1] C. L. Bradley, D. J. Diner, F. Xu, M. Kupinski, and R. A. Chipman, "Spectral invariance hypothesis study of polarized reflectance with the ground-based multiangle SpectroPolarimetric imager," *IEEE Trans. Geosci. Remote Sens.*, vol. 57, no. 10, pp. 8191–8207, Oct. 2019.

[2] P. Curran, "The relationship between polarized visible light and vegetation amount," *Remote Sens. Environ.*, vol. 11, pp. 87–92, Jan. 1981.

[3] P. J. Curran, "A photographic method for the recording of polarised visible light for soil surface moisture indications," *Remote Sens. Environ.*, vol. 7, no. 4, pp. 305–322, Oct. 1978.

[4] S. Liu, B. Yang, Z. Zhang, Y. Xiang, T. Wu, Y. Zhao, and F. Zhang, "Influence of polarized reflection on airborne remote sensing of canopy foliar nitrogen content," *Int. J. Remote Sens.*, vol. 41, no. 13, pp. 4879–4900, Jul. 2020.

[5] B. Yang, Y. Knyazikhin, Y. Lin, K. Yan, C. Chen, T. T. Park, S. Choi, M. Mõttus, M. Rautiainen, R. B. Myneni, and L. Yan, "Analyses of Impact of Needle Surface Properties on Estimation of Needle Absorption Spectrum: Case Study with Coniferous Needle and Shoot Samples," *Remote Sens.*, vol. 8, no. 7, pp. 563–579, Jul. 2016.

[6] Z. Sun, D. Wu, Y. Lv, and S. Lu, "Optical properties of reflected light from leaves: A case study from one species," *IEEE Trans. Geosci. Remote Sens.*, vol. 57, no. 7, pp. 4388–4406, Jul. 2019.

[7] M. Shibayama, T. Sakamoto, and A. Kimura, "A multiband polarimetric imager for field crop survey:—Instrumentation and preliminary observations of heading-stage wheat canopies—," *Plant Prod. Sci.*, vol. 14, no. 1, pp. 64–74, Jan. 2011.

[8] W. Chen, S. Bai, D. Wang, H. Zhao, H. Sun, L. Yi, H. Zhao, D. Xie, J. Peltoniemi, and Z. Li, "Aerosol-induced changes in sky polarization pattern: Potential hint on applications in polarimetric remote sensing," *Int. J. Remote Sens.*, vol. 41, no. 13, pp. 4963–4980, Jul. 2020.

[9] D. Xie, T. Cheng, W. Zhang, J. Yu, X. Li, and H. Gong, "Aerosol type over east asian retrieval using total and polarized remote sensing," *J. Quant. Spectrosc. Radiat. Transf.*, vol. 129, pp. 15–30, Nov. 2013.

[10] B. Y. Ge, X. Mei, Z. Li, W. Hou, Y. Xie, Y. Zhang, H. Xu, K. Li, and Y. Wei, "An improved algorithm for retrieving high resolution fine-mode aerosol based on polarized satellite data: Application and validation for POLDER-3," *Remote Sens. Environ.*, vol. 247, Sep. 2020, Art. no. 111894.

[11] F.-M. Breon, D. Tanre, P. Lecomte, and M. Herman, "Polarized reflectance of bare soils and vegetation: Measurements and models," *IEEE Trans. Geosci. Remote Sens.*, vol. 33, no. 2, pp. 487–499, Mar. 1995.

[12] G. Rondeaux and M. Herman, "Polarization of light reflected by crop canopies," *Remote Sens. Environ.*, vol. 38, no. 1, pp. 63–75, Oct. 1991.

[13] D. Xie, T. Cheng, Y. Wu, H. Fu, R. Zhong, and J. Yu, "Polarized reflectances of urban areas: Analysis and models," *Remote Sens. Environ.*, vol. 193, pp. 29–37, May 2017.

[14] D. J. Diner, F. Xu, M. J. Garay, J. V. Martonchik, B. E. Rheingans, S. Geier, A. Davis, B. R. Hancock, V. M. Jovanovic, M. A. Bull, K. Capraro, R. A. Chipman, and S. C. McClain, "The airborne multiangle SpectroPolarimetric imager (AirMSPI): A new tool for aerosol and cloud remote sensing," *Atmos. Meas. Techn.*, vol. 6, no. 8, pp. 2007–2025, Aug. 2013.

[15] P. Litvinov, O. Hasekamp, and B. Cairns, "Models for surface reflection of radiance and polarized radiance: Comparison with airborne multi-angle photopolarimetric measurements and implications for modeling top-of-atmosphere measurements," *Remote Sens. Environ.*, vol. 115, no. 2, pp. 781–792, Feb. 2011.

[16] F. Waquet, J.-F. Léon, B. Cairns, P. Goloub, J.-L. Deuzé, and F. Auriol, "Analysis of the spectral and angular response of the vegetated surface polarization for the purpose of aerosol remote sensing over land," *Appl. Opt.*, vol. 48, no. 6, pp. 1228–1236, 2009.

[17] F. Maignan, F.-M. Bréon, E. Fédèle, and M. Bouvier, "Polarized reflectances of natural surfaces: Spaceborne measurements and analytical modeling," *Remote Sens. Environ.*, vol. 113, no. 12, pp. 2642–2650, Dec. 2009.

[18] F. Nadal and F.-M. Breon, "Parameterization of surface polarized reflectance derived from POLDER spaceborne measurements," *IEEE Trans. Geosci. Remote Sens.*, vol. 37, no. 3, pp. 1709–1718, May 1999.

[19] B. Yang, H. M. Zhao, and W. Chen, "Modeling polarized reflectance of snow and ice surface using POLDER measurements," (in English), *J. Quantum Spectrosc. Radiat. Transf.*, vol. 236, pp. 106578–106585, Oct. 2019.

[20] Y. He, B. Yang, H. Lin, and J. Zhang, "Modeling polarized reflectance of natural land surfaces using generalized regression neural networks," *Remote Sens.*, vol. 12, no. 2, p. 248, Jan. 2020.

[21] B. Yang, H. Zhao, and W. Chen, "Semi-empirical models for polarized reflectance of land surfaces: Intercomparison using space-borne POLDER measurements," *J. Quant. Spectrosc. Radiat. Transf.*, vol. 202, pp. 13–20, Nov. 2017.

[22] F.-M. Breon and F. Maignan, "A BRDF–BPDF database for the analysis of Earth target reflectances," *Earth Syst. Sci. Data*, vol. 9, no. 1, pp. 31–45, Jan. 2017.

[23] Y. Li, Y. Chen, and J. Huang, "An approach to improve leaf pigment content retrieval by removing specular reflectance through polarization measurements," *IEEE Trans. Geosci. Remote Sens.*, vol. 57, no. 4, pp. 2173–2186, Apr. 2019.
[24] V. Vanderbilt and L. Grant, "Plant canopy specular reflectance model," *IEEE Trans. Geosci. Remote Sens.*, vol. GE-23, no. 5, pp. 722–730, Sep. 1985.
[25] J. Suomalainen, T. Hakala, E. Puttonen, and J. Peltoniemi, "Polarised bidirectional reflectance factor measurements from vegetated land surfaces," *J. Quant. Spectrosc. Radiat. Transf.*, vol. 110, no. 12, pp. 1044–1056, Aug. 2009.
[26] G. Safont, A. Salazar, L. Vergara, and A. Rodríguez, "Nonlinear estimators from ICA mixture models," *Signal Process.*, vol. 155, pp. 281–286, Feb. 2019.
[27] L. Qie, Z. Li, X. Sun, B. Sun, D. Li, Z. Liu, W. Huang, H. Wang, X. Chen, W. Hou, and Y. Qiao, "Improving remote sensing of aerosol optical depth over land by polarimetric measurements at 1640 nm: Airborne test in North China," *Remote Sens.*, vol. 7, no. 5, pp. 6240–6256, May 2015.
[28] J. Chowdhary, B. Cairns, M. Mishchenko, and L. Travis, "Retrieval of aerosol properties over the ocean using multispectral and multiangle photopolarimetric measurements from the research scanning polarimeter," *Geophys. Res. Lett.*, vol. 28, no. 2, pp. 243–246, Jan. 2001.
[29] Z. Li, W. Hou, J. Hong, F. Zheng, D. Luo, J. Wang, X. Gu, and Y. Qiao, "Directional polarimetric camera (DPC): Monitoring aerosol spectral optical properties over land from satellite observation," *J. Quant. Spectrosc. Radiat. Transf.*, vol. 218, pp. 21–37, Oct. 2018.
[30] B. Fougnie, T. Marbach, A. Lacan, R. Lang, P. Schlüssel, G. Poli, R. Munro, and A. B. Couto, "The multi-viewing multi-channel multi-polarisation imager—Overview of the 3MI polarimetric mission for aerosol and cloud characterization," *J. Quant. Spectrosc. Radiat. Transf.*, vol. 219, pp. 23–32, Nov. 2018.
[31] J. Suomalainen, T. Hakala, J. Peltoniemi, and E. Puttonen, "Polarised multiangular reflectance measurements using the finnish geodetic institute field goniospectrometer," *Sensors*, vol. 9, no. 5, pp. 3891–3907, May 2009.
[32] Y. Lu, Y. Zhou, Y. Liu, Z. Mao, W. Qian, M. Wang, M. Zhang, J. Xu, S. Sun, and P. Du, "Using remote sensing to detect the polarized sunglint reflected from oil slicks beyond the critical angle," *J. Geophys. Res., Oceans*, vol. 122, no. 8, pp. 6342–6354, Aug. 2017.
[33] J. I. Peltoniemi, J. Järvinen, N. Zubko, and M. Gritsevich, "Spectropolarimetric characterization of pure and polluted land surfaces," *Int. J. Remote Sens.*, vol. 41, no. 13, pp. 4865–4878, Jul. 2020.

SIYUAN LIU received the B.S. degree in surveying and mapping engineering from the China University of Geosciences, Beijing, China, in 2017. He is currently pursuing the Ph.D. degree in photogrammetry and remote sensing with the School of Earth and Space Sciences, Peking University, Beijing.

His research interests include modeling and applications of optical polarized remote sensing and vegetation remote sensing.

LEI YAN (Senior Member, IEEE) received the B.E. degree from the Nanjing University of Aeronautics and Astronautics, Nanjing, China, in 1982, the M.E. degree from the Naval University of Engineering, Nanjing, in 1989, and the Ph.D. degree from Tsinghua University, Beijing, China, in 1994.

From 1998 to 2000, he was a Full Professor and an Academic Leader of the One Hundred Famous Scientists Plan at the Changchun Institute of Optics, Fine Mechanics and Physics, Chinese Academy of Sciences, Changchun, China. Since 2001, he has been a Professor and the Head of the Beijing Key Laboratory of Spatial Information Integration and Its Applications, School of Earth and Space Sciences, Institute of Remote Sensing and Geographic Information System, Peking University, Beijing. He has authored six books, over 200 articles, and 19 patents. His major research interests include digital imaging, airborne remote sensing systems and image processing, and optical polarized remote sensing.

Dr. Yan was a recipient of the First Award for Technology Invention of Beijing City, in 2019, and the Second Award for National Technology Invention, in 2015, for his contribution on the mechanism and theory and wide applications of optical polarized remote sensing.

BIN YANG (Member, IEEE) received the Ph.D. degree in photogrammetry and remote sensing from the School of Earth and Space Sciences, Peking University, Beijing, China, in 2017.

Since 2017, he has been an Assistant Professor with the College of Electrical and Information Engineering, Hunan University, Changsha, China, and the Key Laboratory of Visual Perception and Artificial Intelligence of Hunan Province, Changsha. His research interests include remote sensing and artificial intelligence.